Journal of Material and Process Technologies

Available online at http://journal.aastu.edu.et/

# Petro-stratigraphy and Geochemistry of volcanic rocks from the eastern escarpment of Main Ethiopian Rift

*Solomon Tadesse [1,2,3], Takele Chekol[1, 2, *], Daniel Meshesha [1, 2], Bedru Hussien[1, 2]*

[1]*Department of Geology, College of Applied Sciences, Addis Ababa Science and Technology University, P.O. Box 16417, Addis Ababa, Ethiopia*
[2]*Mineral Exploration, Extraction and Processing Center of Excellence, Addis Ababa Science and Technology University, P.O. Box 16417, Addis Ababa, Ethiopia.*
[3]*Present address: Wolaita Sodo University, Wolaita Sodo, Ethiopia.*

Article Information

*Article history:*
Received 25 April 2025
Received in revised form 05 June 2025
Accepted 10 June 2025

Keywords:
Dera-Sire
Basalt
Ignimbrite
OIB-like
E-MORB

*Corresponding author.*
*E-mail: takele.chekol@aastu.edu.et (T. Chekol)*
https://doi.org/10.69660/jmpt.v2i1.114

**Abstract**

The Dera-Sire section is located in the eastern escarpment of the Central Main Ethiopian Rift. The section consists of, from bottom to top, lower flood basalt (Oligocene), lower ignimbrite, tuff and ash, upper basalt (Pliocene), and upper ignimbrite. The lower flood basalts are characterized by phyric to aphyric textures. The lower and upper ignimbrite units contain crystals of quartz, plagioclase, and lithic fragments embedded within a glassy groundmass. The upper basalts are aphyric to plagioclase phyric in texture. The lower flood basalts and upper basalts are alkaline and sub-alkaline (tholeiitic) in composition, respectively. The geochemical variations suggest at least two dominant mantle components that require the production of both upper tholeiitic and lower alkaline basalts. The components are an OIB-like component, which might be similar to the Afar plume composition, and an E-MORB-like component in the asthenosphere, indicating that there were no temporal mantle source variations from Oligocene to Pliocene magma generations. However, the alkaline affinity of the lower flood and tholeiitic nature of the upper basalts suggest that the depth of melting of the lower flood basalt is relatively deeper than that of the upper basalts. The fractionated mineral assemblages of the lower flood basalts (plagioclase-olivine-minor clinopyroxene) and upper basalts (dominant plagioclase with minor clinopyroxene) suggest that the mantle-derived magma rose, accumulated, and fractionated in the lower crustal and upper crustal chambers, respectively. Subsequently, the fractionated magma from the lower and upper crustal chambers rose to the surface and produced lower flood basalts and upper basalts, respectively.

## 1. Introduction

East African volcanism dates back to approximately 45 Ma [1-3], preceding the formation of the East African Rift System (EARS) by approximately 20 million years [4-6]. Volcanic activity in the region is linked to the activity of mantle plumes (e.g. Ebinger and Sleep [7], George et al. [3], Rogers et al. [8], Furman et al.[9], Rogers [10] and Pik et al.[11]), which has a significant impact on the geological history of the area during various periods. The Ethiopian volcanic province, the northern part of the EARS, is a large igneous province (LIPs) covering an area of approximately 600,000 km$^2$ [6, 12-14]. The Ethiopian volcanic series consists of two major categories: 1) Continental Flood Basalt (CFB) together with shield volcanoes, which have extensively covered the northwestern and southeastern plateaus of the country; and 2) rift volcanism that includes volcanic activity along the Afar Rift and the Main Ethiopian Rift (MER).

Most of the Ethiopian CFB erupted around 30 Ma to form a vast volcanic plateau within a short period of <5 Myr [5, 15-18]. During the Miocene, the continental flood basalts were overlain by the eruptions of massive shield volcanoes (for example, Mts. Megezez, Guguftu, Guna, Simien, and Choke) ~ 23–10 Ma [6, 13, 18, 19]). The MER, the northern part of the EARS, stretches approximately 1000 km and represents the region between the Kenya rift and the Afar triple junction (Figure 1(a)), where extensional deformation began to develop from the late Oligocene-early Miocene to the present (e.g., Ebinger et al.[2], Woldegabriel et al.[20], Ebinger et al.[7], Wolfenden et al. [21]). The MER system is characterized by a long history of magmatism associated with different degrees of lithospheric extension. Based on the structural features of the rift segments, the MER is divided into three main segments: the Northern MER, Central MER, and Southern MER, reflecting the different stages of the continental extension process interpreted from different fault architectures, timing of volcanism, and deformation [20-22]. The study area is located in the Central MER, which is relatively young and formed less than 8 Ma after the formation of the Northern MER [23]. The volcanic activity in this region is bimodal in composition, with a prevalence of silicic products [18] (Figure 1(b)).

Most previous studies on Ethiopian volcanism, particularly the rift margin, have been conducted at a regional scale, and detailed studies on single sections of the rift margin are limited. Several parts of the Ethiopian Plateau and rift volcanic rocks need detailed and all-inclusive studies in terms of lithologic unit identification, lithological extent, and textural and mineralogical characteristics, and finally to establish a complete stratigraphic section. The investigated area (Figure 1), which is the eastern escarpment of the central MER and the western boundary of the southeastern Ethiopian Plateau, hosts both flood basalts (Oligocene) and

rift volcanic rocks, including basalts and pyroclasts (Pliocene) [24]. This study focuses on an area located between the towns of Dera and Sire, covering a 900-meter stratigraphic section from the Keleta River valley (1580m) to the top of the escarpment (2480m). It is an interesting area to investigate the petro-stratigraphy and geochemical nature of volcanic rocks. Therefore, this study aims to understand the petro-stratigraphy and geochemical characteristics of volcanic rocks and presents new data related to petrography, petrology, and geochemistry.

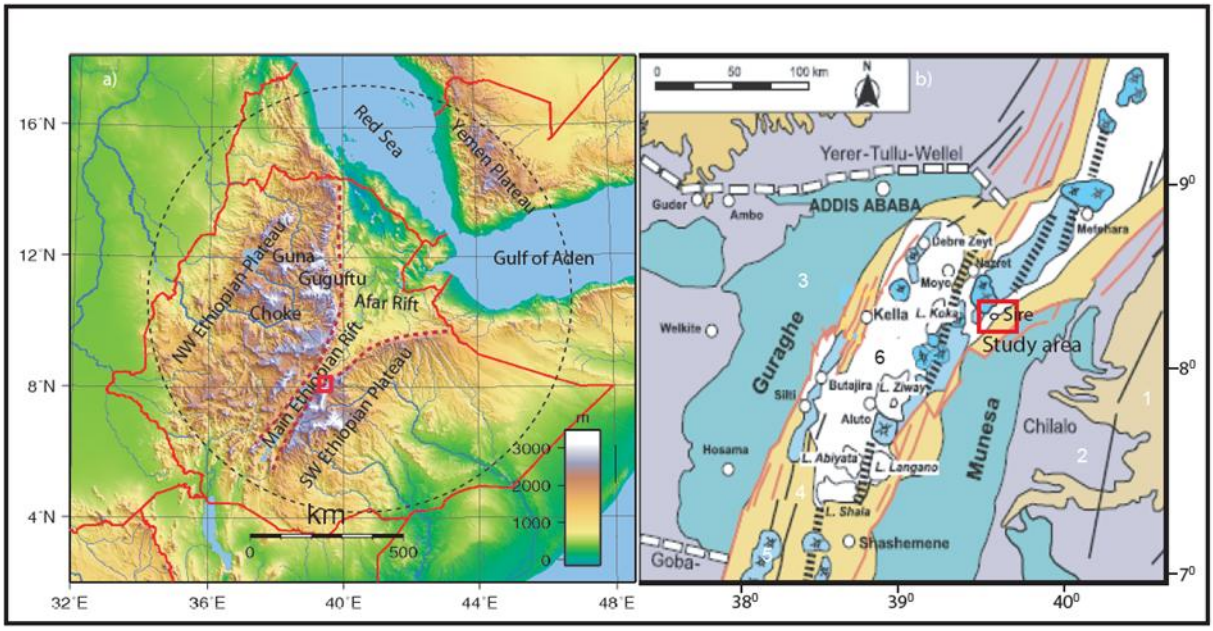


Fig. 1 a) Digital Elevation map of Ethiopia and part of Yemen showing the position of the Main Ethiopia Rift, Gulf of Aden, Red Sea, Ethiopian and Yemeni Plateau, including the distribution of shield volcanoes (Kieffer et al., 2004; Corti, 2009) and b) Simplified geological map of central MER after Jepsen and Athearn (1997). 1)Pre-Tertiary sediments and crystalline basement, 2) Oligocene (32–29 Ma) and lower Miocene (12–8 Ma) plateau volcanic, 3) Miocene–Pliocene rift-shoulder trachytic-rhyolitic volcanic and pyroclastic layers, 4) Plio-Pleistocene rift floor, 5) Quaternary central volcanic and basaltic lava flows, associated scoria cones and phreato-magmatic deposits, and 6) Quaternary lacustrine sediments and interbedded pyroclastics.

## 2. Regional geological setting

The earliest volcanic activity in the EARS occurred between 40 and 45 million years ago in southwestern Ethiopia and northern Kenya [1-3], However, extensive and widespread volcanism in Ethiopia, Eritrea, and Yemen commenced between 31 and 22 Ma, during which the CFB and their associated felsic pyroclastic rocks and lavas erupted [4-6, 15, 16, 25]. Subsequently, from 30 to 10 Ma, a number of large shield volcanoes erupted on the surface of the volcanic plateau [6, 13, 18, 19]. In general, plateau uplift, crustal thinning, rifting, and formation of magmatic provinces during the evolution of the EARS are attributed to the upwelling of mantle plumes [3, 7-11]. The EARS is a Miocene-Quaternary intra-continental extensional system composed of several interacting rift segments extending from Mozambique in the south to Ethiopia-Afar in the north [26-30]. The EARS joins the Gulf of Aden and Red Sea Rifts at the Afar triple junction (Figure 1(a)). The Rift System enables the study of compositional variation of erupted magmas as a function of extension [31].

The Ethiopian volcanic province is suggested to be related to Afar mantle plume impingement, uplift, volcanism, and extension (e.g., Woldegabriel et al. [20], George et al.[3], Ebinger and Sleep [7], Rogers et al. [8], Furman et al. [9], Rogers [10], and Pik et al. [11]). In northern and central Ethiopia, volcanism began during the Oligocene with eruptions of thick successions of the CFB and their associated felsic pyroclastic rocks and lavas. Most of these flood basalts erupted within a short period of time (< 5 Ma), where the bulk of the flood basalts extruded between 31 and 29 Ma, predating the main extensional event in the Ethiopian rift [4, 5, 15, 16, 32]. However, the earliest lavas in the Ethiopian Province were found in southern Ethiopia, dating to 45-35 Ma [1, 18, 33]. The MER is an 80-kilometre-wide rift zone that separates the uplifted northwestern and southeastern Ethiopian plateaus [12]. (Figure 1). The MER extensional deformation begins to develop in the late Oligocene–early Miocene with a rate of extension of 6-7 mm/yr (e.g., Chernet et al. [34], Ebinger et al. [35], and Bonini et al. [36]). The majority of MER volcanics are Plio-Quaternary in age, with older volcanics restricted to the rift margins. Magmatic activity appears to have been episodic rather than continuous [20, 34, 37].

## 3. Materials and methods

Petrographic studies were carried out on 20 representative fresh samples from different volcanic units of the Dera-Sire section. Thin sections were prepared at the Central Laboratory of the Geological Institute of Ethiopia (GIE). The thin sections were examined using a standard petrographic microscope at the petrography laboratory of the Geology Department, Natural and Applied Science College, Addis Ababa Science and

Technology University (AASTU).

Whole-rock geochemical analyses of seven representative samples from the basalts were performed using X-ray fluorescence (XRF) for major and trace elements at the Geochemical and Geophysical Laboratory Center of Arba Minch University. Sample preparation for geochemical analysis began by removing the weathered part from the rock surface. The sample was then crushed into millimetre-sized chips using a jaw crusher. The chips were carefully handpicked using a stereomicroscope to avoid the phenocryst, and then pulverized to the size of the powder that passed through a 200 mesh with an alumina ceramic mill at the GIE. The powdered samples were submitted to the geochemical and geophysical laboratory center of Arba Minch University for major and trace element geochemical analyses. To evaluate the precision and degree of accuracy, blank, duplicate, and standard samples were analyzed and compared with previously analyzed standard results. Loss of Ignition (LOI) analysis was performed at the Laboratory Center of Analytical Chemistry, Arba Minch University. The prepared sample (1.0 g) was placed in an oven at 1000 ◦C for 1 h, cooled, and then weighed (this method of sample decomposition is called thermal decomposition furnace (TGA)). The percent loss on ignition was calculated from the difference in weight.

## 4. Results

### 4.1. Lithology and petrography of the study area

The study area in the eastern escarpment of the Central MER covers the volcanic rocks of the Dera-Sire section. It has a 900-meter-thick volcanic sequence from the base of the Keleta River (1580 m a.s.l.) to the top of the escarpment (2480 m a.s.l.) (Figs. 1 and 2). The lithological units were described according to their stratigraphic succession (Fig. 2) based on their vertical contact relationship in the field and information from previous absolute age data (Agostini et al., 2011). The lithological units recognized in the study area from the bottom to the top of the stratigraphy include lower basalt (Oligocene); lower ignimbrite, tuff, and volcanic ash; upper basalt (Pliocene); and upper ignimbrite (Figure 2).

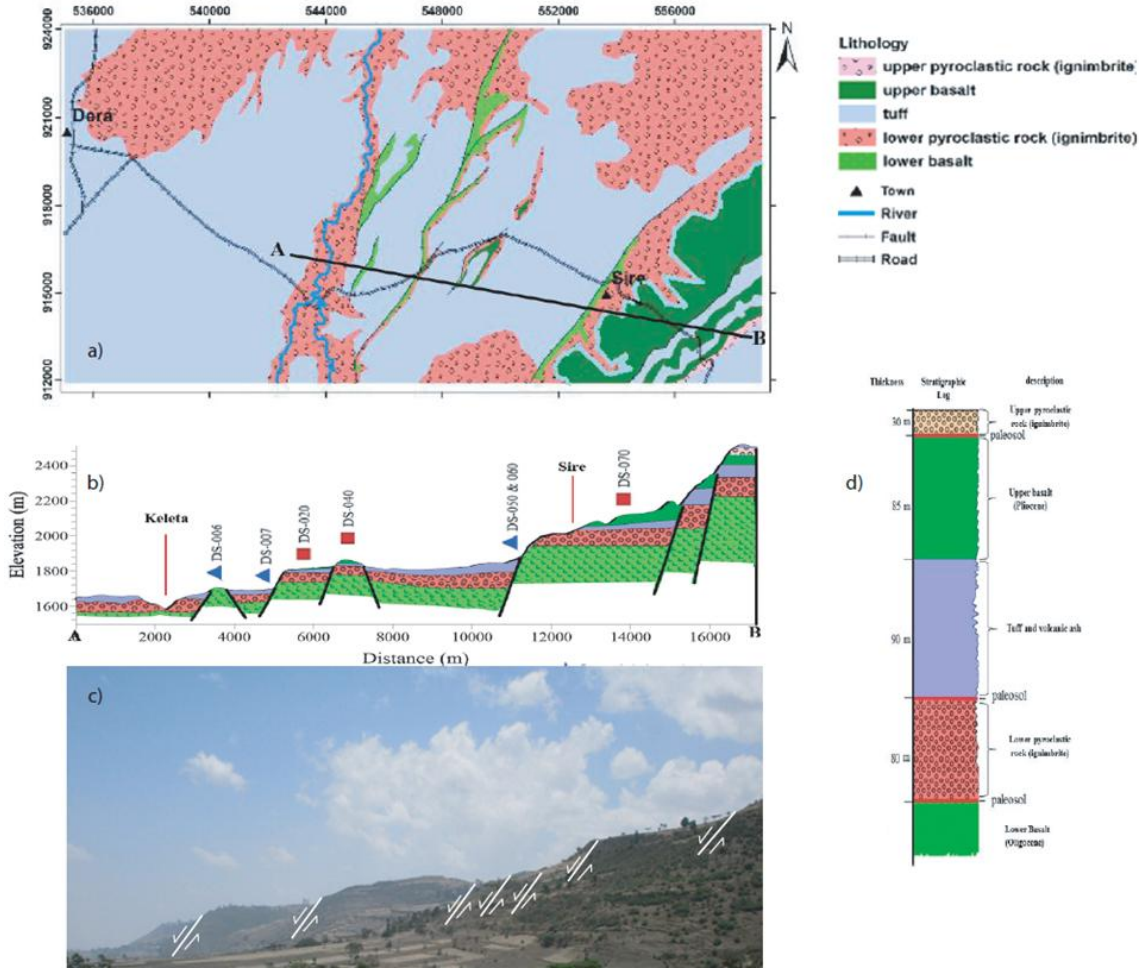


Figure 2 a) Geological map of the Dera-Sire area, b) Cross-section of the Dera-Sire area along profile line A-B. Vertical exaggeration (2x), c) Panoramic view of the eastern escarpment showing a series of step faults on the eastern rift escarpment and d) Stratigraphic log of the Dera-Sire volcanic section with its vertical thickness.

Journal of Material and Process Technologies

Available online at http://journal.aastu.edu.et/

**Lower basalt**: The lower basalt is Oligocene in age [24], and is mainly exposed in the western and central parts of the study area (Figure 2). It typically formed steep to moderately gentle topographic features (Figure 3 (a and b). The lower basalt is dark gray, massive, and in places, vesicular. The vesicles are partially filled with calcite and silica. In some places, it is well exposed and shows sharp contact with the overlying ignimbrite unit. The basalt is generally porphyritic and is characterized by a dominant and large-sized phenocryst of plagioclase. The lower basalt is not a monotonous unit, but consists of several lava flows separated by 30-40 cm reddish brown paleosols (Figure 3 (a and b)). Petrographically, the lower basalt is phyric in texture. The modal percentages of the phenocryst are 2-5% plagioclase, 1-3% olivine, and 0-1% clinopyroxene. The plagioclase phenocrysts are euhedral and tabular in shape, showing zoning and twinning. The olivine phenocrysts are subhedral to unhedral in shape and are partly altered to iddingsite. The groundmass is composed of microcrystalline plagioclase laths, olivine, clinopyroxene, and opaque minerals. Generally, the lower basalt is plagioclase-olivine phyric basalt and holocrystalline in texture (Figure 3 (c-e)).

**Lower ignimbrite: -** The lower ignimbrite unit is exposed around the Keleta River, and the Rift margin overlays the lower basalt, reaching an overall thickness of ~80 m (Figure 2). The lower ignimbrite is composed of a sequence of ignimbrite layers separated by paleosols (Figure 4a). It is composed of lithic fragments with a maximum diameter of 3 cm (Figure 4b). Around the Keleta River, the ignimbrite consists of well-welded dark ignimbrite with "fiamme" and gray ignimbrite with a dominant presence of rock fragments (Figure 4a). Petrographically, the lower ignimbrite contains quartz, plagioclase, alkali feldspars (sanidine and orthoclase) crystals, and lithic fragments embedded within a glassy groundmass (vitric texture) (Fig. 4c and d). The modal abundances are 2% lithic fragments, ~1% quartz, < 1% plagioclase, and alkali feldspars. The quartz grains are subhedral to round in shape. The lithic fragments are angular to subrounded. The plagioclase and alkali feldspars are elongated in shape. The lithic fragments are composed of basaltic fragments (Figure 4c), and the matrix is composed of glass shards.

**Tuff and ash: -**The tuff and ash unit covered an extensive area and formed a gentle slope (Figs. 2a, b, and d, and 6a and b). The ash and tuff are found intercalated in most exposures (Fig. 6b). The ash varies from a thin layer up to 2 m thick, is characterized by a light grayish color, and is composed of pumice fragments. The tuff and ash conformably overlie the lower ignimbrite unit.

**Upper basalt: -**The upper basalt is Pliocene in age [24] and is distributed in the central and southeastern parts of the study area, exposed along the Kara, Sire, and Bollo localities (Figure 2a). The upper basalt forms a steep to moderately gentle topography (Fig. 2b), and in places, it has columnar joints. The overall estimated thickness of this unit is ~ 85 m (Figure 2d). It conformably overlies the tuff and ash and is separated from the upper ignimbrite by a paleosol (Figure 6c). It is dark to dark gray, with aphanitic to porphyritic, scoriaceous, and vesicular textural varieties (Figure 5a and b). The porphyritic variety of the upper basalt is characterized by visible plagioclase phenocrysts.

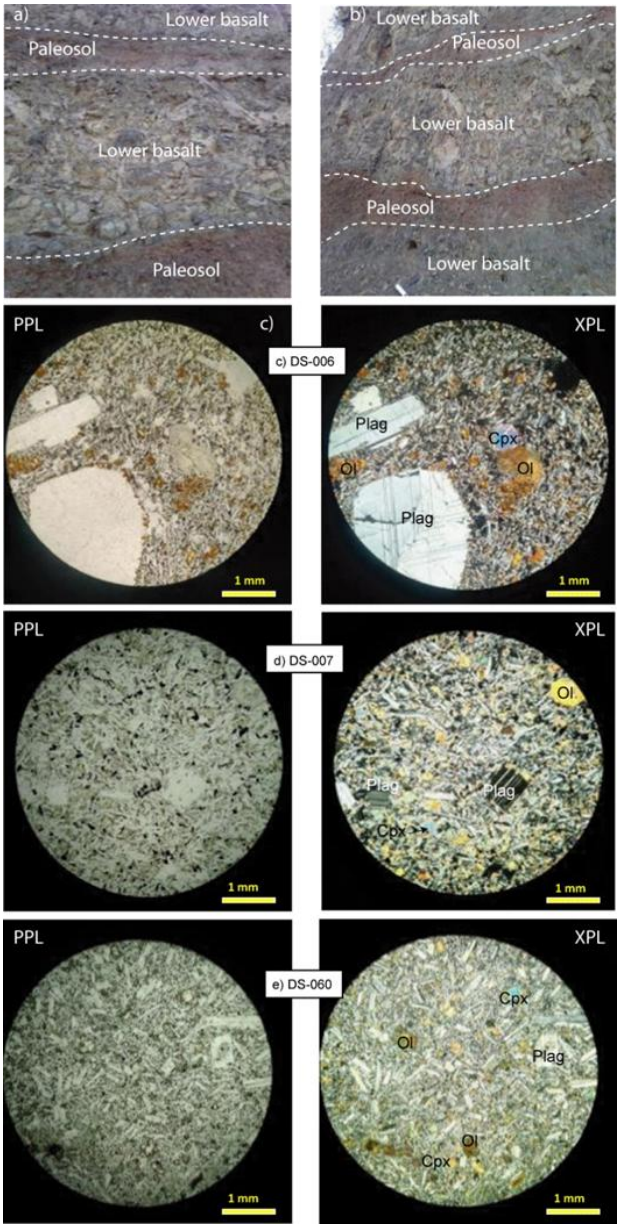


Figure 3. Outcrops and selected representative photomicrographs of the lower flood basalts a) and b) lava flow separated by paleosols c) and d) plagioclase-olivine phyric basalt and e) sparsely phyric basalts. In Plane Polarized Light (PPL) and Cross-polarize (XPL). 4X magnification.

Petrographically, the upper basalt is aphyric to sparsely phyric in texture. The modal percentages of the phenocryst are 2-6% plagioclase and 0-1%

clinopyroxene and 0-1% olivine. The groundmass is composed of microcrystalline plagioclase laths, olivine, clinopyroxene, and opaque minerals. Generally, the upper basalt is sparsely plagioclase phyric to aphric basalt and holocrystalline and intergranular in texture (Figure 5c-e).

**Upper ignimbrite: -**The upper ignimbrite unit is exposed at the top of the rift escarpment and separated from the upper basalt by a 30–50 cm thick layer of paleosol (Figs. 2 and 6c). The overall thickness of this ignimbrite is approximately 30 m (Fig. 2d). In some places, ignimbrite is intercalated with thin layers of tuff and ash. The ignimbrite contains fiamme, mineral crystals, and lithic fragments.

Petrographically, the upper ignimbrite shows mineral crystals and lithic fragments set in a glassy matrix (glass shards). The mineral crystals are composed of 3% quartz and 2% plagioclase. The lithic fragments are mostly basaltic and pumice. The basaltic fragments are composed of altered olivine (iddingsite) and opaque minerals (Fig. 6d).

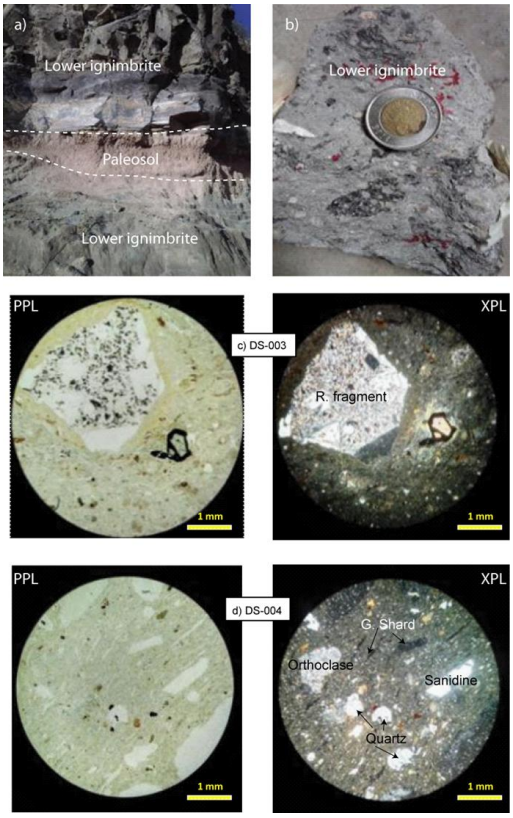


Figure 4. Outcrops and selected representative photomicrographs of the lower ignimbrites a) ignimbrite layers separated by paleosol, b) rock fragments in the ignimbrite hand specimen, c) glassy textured ignimbrite with large basaltic fragments >2mm in diameter and d) ignimbrite with quartz and lithic fragments. In Plane Polarized Light (PPL) and Cross-polarize (XPL). 4X magnification.

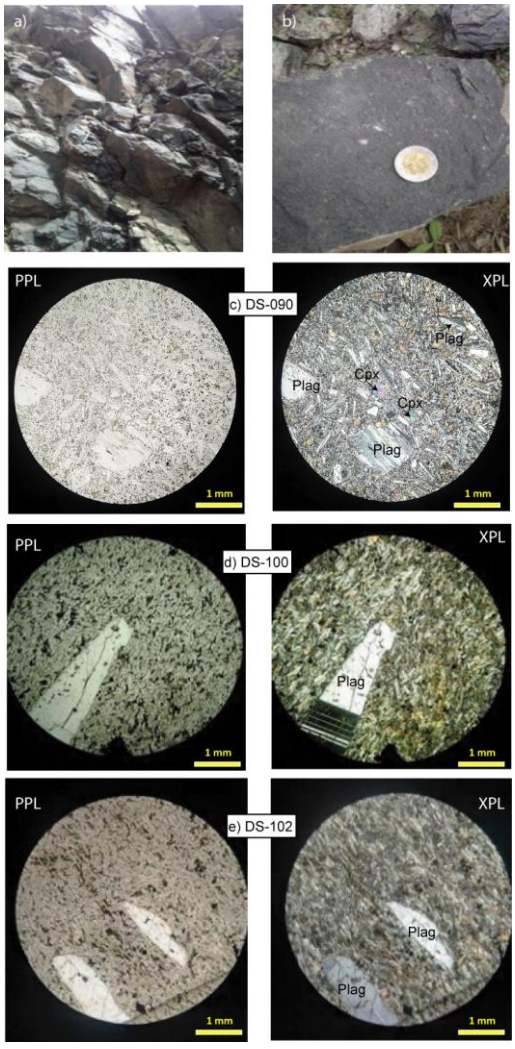


Figure 5. Outcrops and selected representative photomicrographs of the upper basalts. a) outcrops of upper basalts, b) plagioclase phenocrysts in the upper basalts, c) and d) phyric texture of upper basalts and e) sparsely phyric upper basalts. In Plane Polarized Light (PPL) and Cross-polarize (XPL). 4X magnification.

**Whole-rock major elements: -**The whole-rock major element data for representative basalt samples from the Dera-Sire section are listed in Table 1. In the total alkali-silica (TAS) classification diagram of Le Bas et al. (1986), all the analyzed samples fall in the field of basalt and are subdivided into transitional to alkaline and tholeiite series (Figure 7). As shown in Figure 7, the Oligocene lower flood basalts are an alkaline series with transitional affinity and plot closer to the western rift wall basalts [38] and Miocene alkali western rift basalts [39]. The Pliocene upper basalts are a tholeiitic series and plot with some samples of the eastern rift basalts [38] .

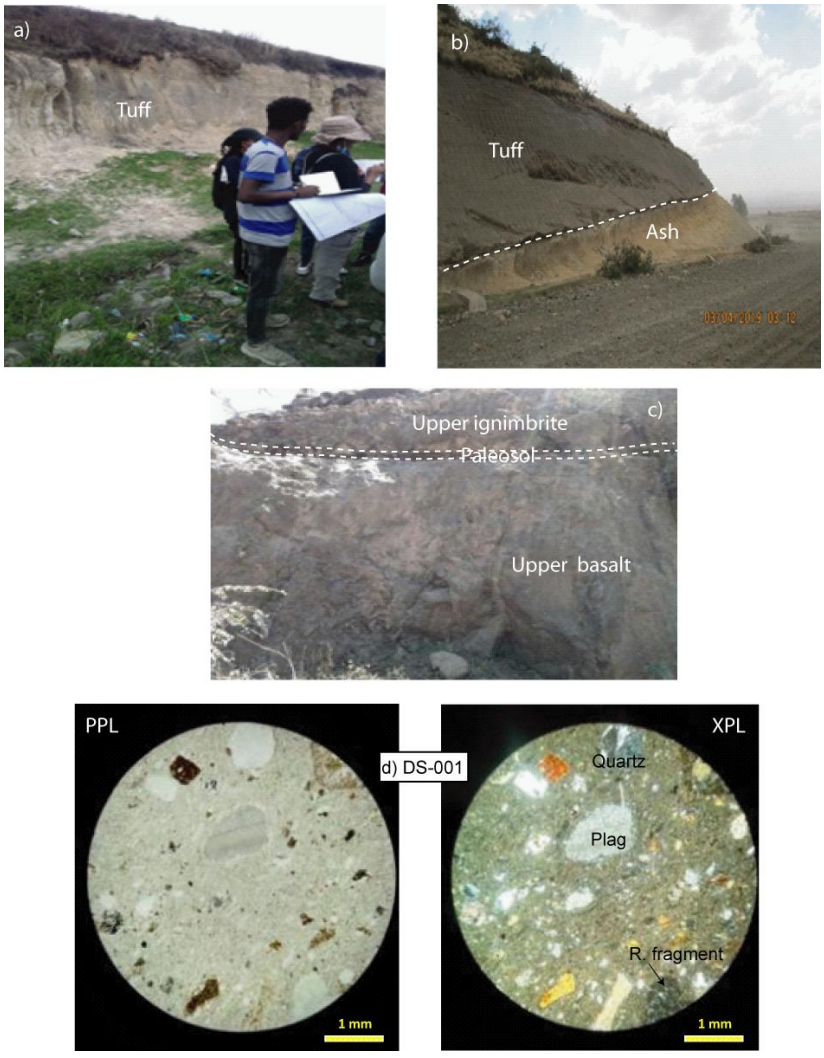


Figure 6. Outcrops of a) tuff, b) tuff and ash, c) upper basalts and upper ignimbrite separated by paleosol and d) selected representative photomicrograph of upper ignimbrite with crystal and lithic fragments set in a glassy matrix. In Plane Polarized Light (PPL) and Cross-polarize (XPL). 4X magnification.

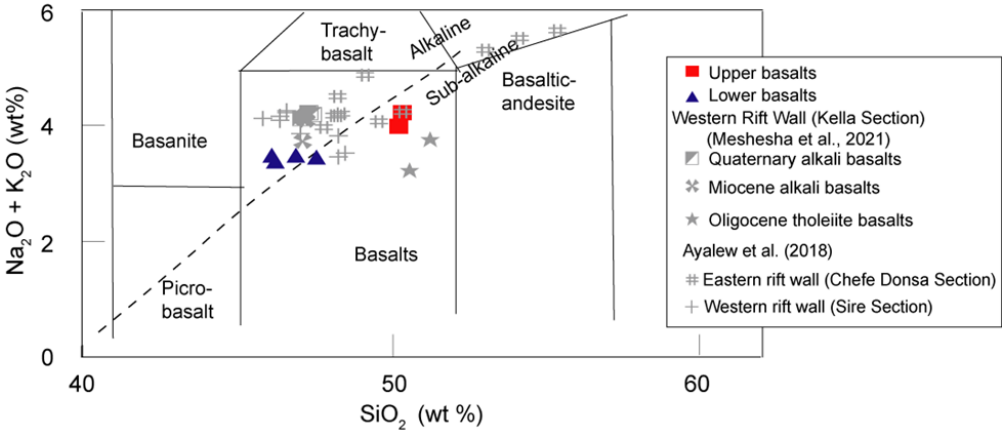


Figure 7. Total alkali ($Na_2O + K_2O$) versus $SiO_2$ diagram [40] of the upper and lower basalts. Data for Western (Chefe Donsa Section) and Eastern Rift Wall (Sire Section) [38]), Western Rift Wall (Kella Section) [39] are plotted for comparison. The dividing line of alkaline and sub-alkaline is from Irving and Baragar [41].

Journal of Material and Process Technologies

Available online at http://journal.aastu.edu.et/

Table 1. Major and trace element data for basalts from Dera-Sire Section, eastern escarpment of central Main Ethiopian Rift.

| Sample | Lower basalts | | | | Upper basalts | | |
|---|---|---|---|---|---|---|---|
| | DS-006 | DS-007 | DS-050 | DS-060 | DS-020 | DS-040 | DS-070 |
| $SiO_2$ (wt. %) | 46.88 | 47.56 | 46.28 | 45.99 | 50.5 | 50.43 | 50.25 |
| $TiO_2$ | 4.14 | 3.83 | 3.98 | 3.89 | 3.5 | 3.53 | 3.5 |
| $Al_2O_3$ | 14.38 | 13.64 | 14.1 | 13.92 | 14.53 | 14.47 | 14.4 |
| $Fe_2O_3$ | 14.65 | 14.94 | 15.37 | 15.43 | 13.53 | 14.04 | 13.73 |
| MnO | 0.13 | 0.23 | 0.15 | 0.21 | 0.22 | 0.18 | 0.17 |
| MgO | 5.5 | 5.37 | 5.9 | 5.9 | 3.08 | 3.4 | 3.6 |
| CaO | 10.06 | 10.03 | 10.03 | 10.12 | 9.23 | 9.26 | 9.25 |
| $Na_2O$ | 2.77 | 2.78 | 2.71 | 2.79 | 3.01 | 3 | 3.04 |
| $K_2O$ | 0.71 | 0.67 | 0.67 | 0.7 | 1.21 | 0.98 | 1.15 |
| $P_2O_5$ | 0.74 | 0.92 | 0.78 | 0.74 | 0.88 | 0.87 | 0.87 |
| LOI | 0.61 | 0.7 | 0.47 | 0.93 | 0.5 | 0.73 | 0.77 |
| Total | 99.96 | 99.97 | 99.95 | 99.69 | 99.69 | 100.2 | 99.96 |
| Sc (ppm) | 27.33 | 29.36 | 25.75 | 29.07 | 30.32 | 28.75 | 29.48 |
| V | 409 | 386.95 | 398.25 | 407.08 | 336.79 | 358.4 | 362.79 |
| Ni | 41.6 | 32.56 | 40.8 | 42.71 | 19.53 | 20.53 | 23.6 |
| Rb | 11.07 | 14.15 | 13.93 | 14.38 | 21.42 | 20.58 | 19.51 |
| Sr | 710.72 | 675.53 | 721.54 | 702.64 | 602 | 594.74 | 594.15 |
| Zr | 150.05 | 164.09 | 145.32 | 155.91 | 171.38 | 164.16 | 165.08 |
| Th | 1.68 | 1.95 | 1.69 | 1.75 | 2.14 | 2.09 | 2.09 |
| Ba | 453.55 | 734.06 | 477.98 | 459.94 | 712.96 | 712.36 | 677.76 |
| Zn | 101.71 | 125.75 | 106.24 | 107.06 | 127.17 | 90.3 | 95.14 |
| Cu | 99.61 | 144.54 | 143.72 | 115.23 | 75.39 | 95.74 | 67.15 |
| Cr | 15.42 | 16.13 | 29.95 | 33.26 | 53.21 | 46.25 | 14.15 |
| W | 54.22 | 57.44 | 50.71 | 48.38 | 50.12 | 40.51 | 45.35 |
| Pb | 2.16 | 2.3 | 2.25 | 2.06 | 2.84 | 2.92 | 3.01 |
| Nb | 18.57 | 18.86 | 18.8 | 18.17 | 18.92 | 18.51 | 18.38 |
| Hf | 3.82 | 4.13 | 3.63 | 3.91 | 4.32 | 4.13 | 4.16 |
| Mn | 976.29 | 1723.9 | 1237.76 | 1224.6 | 1693.92 | 1360.91 | 1290.22 |
| Mo | 4.59 | 8.49 | 5.43 | 4.36 | | 10.39 | 4.7 |

The lower basalt shows MgO ranging from 5.37–5.9 wt% and $SiO_2$ ranging from 45.99–47.56 wt%. The upper basalt has a slightly narrow range of MgO and relatively higher $SiO_2$ contents, ranging from 3.08–3.6 wt% and 50.25–50.5 wt%, respectively, compared to the lower basalt. Selected major elements versus MgO (wt%) plots are shown in Figure 8. In most plots, the lower and upper basalts showed two distinct compositions. $TiO_2$, CaO, $Fe_2O_3$, and $CaO/Al_2O_3$ show higher contents in the lower basalt, while $Al_2O_3$, $K_2O$, $Na_2O$, and $SiO_2$ are higher in the upper basalt (Fig. 8a–h). $Al_2O_3$ is positively correlated with MgO in the lower basalt and negatively correlated with MgO in the upper basalt. $Fe_2O_3$ shows positive trends with MgO for both the lower and upper basalts. In the upper basalt, CaO, $TiO_2$, and $Na_2O$ remained almost constant as the MgO content varied. $K_2O$ is constant in the lower basalt but negatively correlated in the upper basalt. The MgO versus $CaO/Al_2O_3$ ratio shows a positive correlation trend in both groups, but the $CaO/Al_2O_3$ ratio defines a gentler and steeper slope in the upper and lower basalts, respectively (Fig. 8h). $CaO/Al_2O_3$ defines two groups between the lower and upper basalts: the lower basalt plots towards the higher $CaO/Al_2O_3$ ratio (> 0.7), while the upper basalt has a ratio of < 0.65.

## Whole-rock trace element: -

Trace element data for the Dera-Sire section basaltic rocks is shown in Table 1. Selected trace elements plotted with MgO are shown in Figure 9. The compatible elements Ni and V are positively correlated with MgO in both Oligocene lower basalts and Pliocene upper basalts. Incompatible element Nb is almost constant with decreasing MgO contents in both the Oligocene lower basalts and Pliocene upper basaltic groups. Zr, Sr, and Th also remain constant as MgO decreases in the upper basaltic group. In the lower basaltic group, while Zr and Th show a negative correlation, Sr shows a positive correlation with MgO. In most of the plots (Fig. 9), the Oligocene lower basalts plotted together or along the same trend with Eastern and Western rift wall basalts (Ayalew et al., 2018) and the western rift wall Oligocene tholeiitic basalts (Meshesha et al., 2021), whereas the plot of the Pliocene upper basalts of this study were isolated.

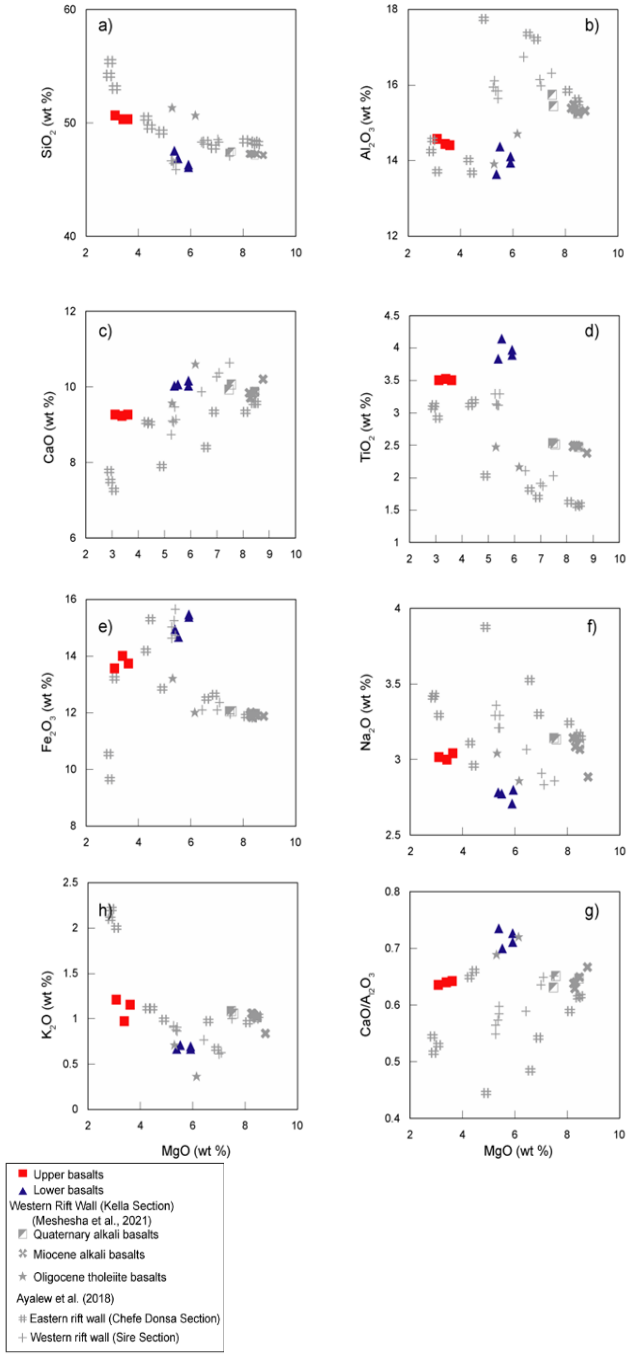


Figure 8 Variation diagram of major elements vs. MgO (wt. %) of samples from upper and lower basalts. Data for Western (Chefe Donsa Section) and Eastern Rift Wall (Sire Section) [38], Western Rift Wall (Kella Section) [39] are plotted for comparison

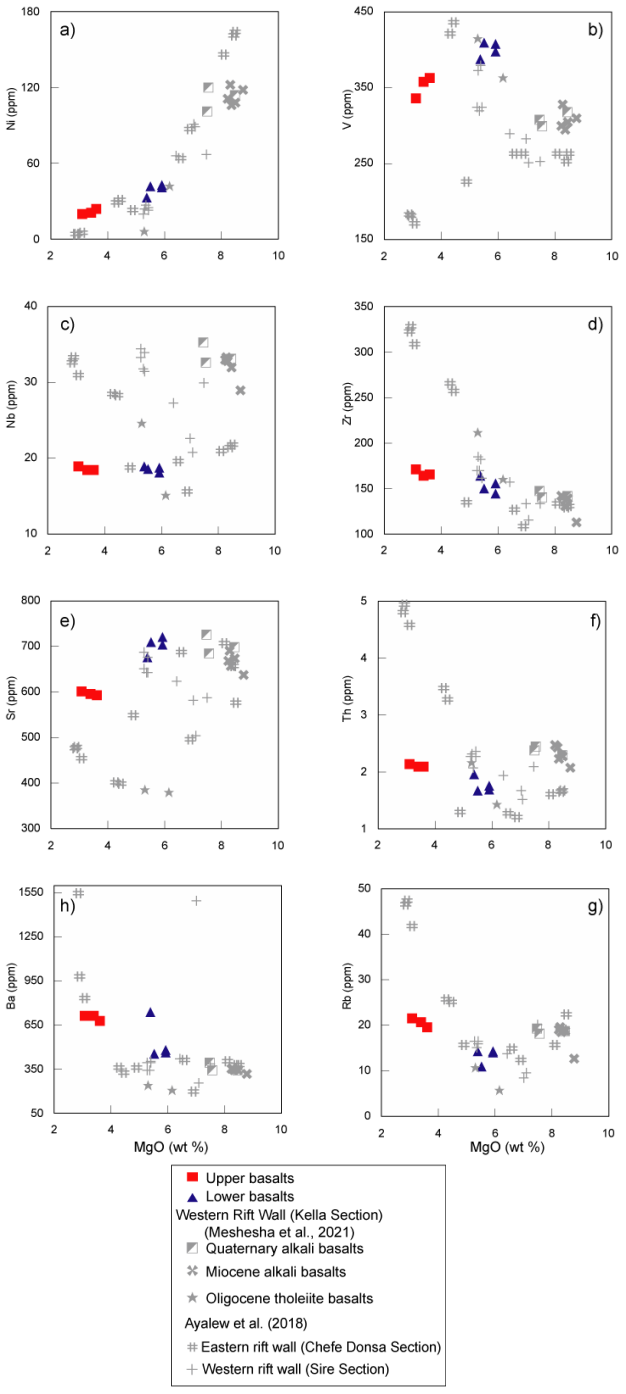


Figure 9. Selected trace element plots against MgO (wt.% %) from upper and lower basalts. Data for Western (Chefe Donsa Section) and Eastern Rift Wall (Sire Section) [38], Western Rift Wall (Kella Section) [39], 2021) are plotted for comparison.

Figures 10 (a and b) show Zr/Nb vs. Rb/Nb and MgO vs. Zr/Nb plots. The Zr/Nb ratio is almost constant in all samples from both Oligocene lower basalts and Pliocene upper basalts. However, the Rb/Nb ratio is higher in the Pliocene upper basalts as compared with the Oligocene lower basalts.

The primitive mantle-normalized multi-element patterns are shown in Figure 10 (c-f). The patterns in both groups are almost similar and show a slight enrichment of highly incompatible elements over relatively less incompatible elements. The overall patterns in both groups show a closer resemblance to oceanic island basalts (OIB type) than to enriched mid-oceanic basalt (E-MORB) and typical normal mid-oceanic basalt (N-MORB) [42]. Although both the lower and upper basalts display a general OIB pattern, they have some different features. There is a significant enrichment in Ba in the lower and upper basalts of the Dera-Sire section compared to the typical characteristic features of oceanic island basalt (OIB) patterns [43]. On the other hand, HFSE (Nb, Zr, and Hf) in both basaltic groups show a slight depletion relative to the OIB pattern. Compared with the western rift wall basalts in the Kella area [39], both the lower and upper basalts in this study bear clear similarities in patterns (Figure 10 d). Furthermore, except for the negative K anomaly observed in the study by Ayalew et al. [38], the Dera-Sire basalt patterns show overall similarities with the eastern and western rift wall basalts (Figure 10 (e and f)).

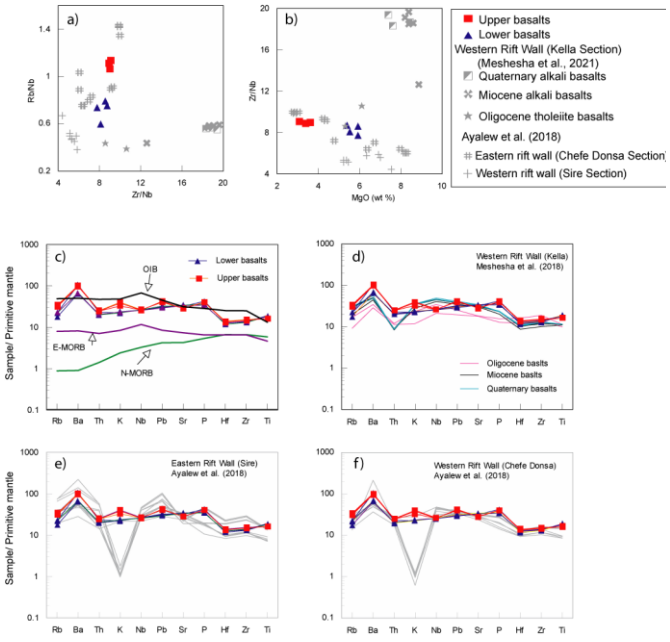


Figure 10 a) Plots of Rb/Nb vs. Zr/Nb, b) MgO vs. Zr/Nb, c) multi-element primitive mantle-normalized patterns of the upper and lower basalts compared with d) Western Rift Wall (Kella; Meshesha et al., 2021), e) Western Rift Wall (Chefe Donsa [38]); and d) Eastern Rift Wall (Sire; [38]). Mantle and normalization values of OIB, E-MORB and N-MORB are from Sun and McDonough [42].

## 5. Discussion

The MER is divided into Southern, Central and Northern Rift Segments [18]. The study area is part of the central segment of the eastern escarpment of the MER, which is characterized by a diverse geology consisting of basalt, ignimbrite, and tuff. The eastern escarpment of the MER in the study area (Dera-Sire section) is highly affected by a series of step-normal faults (Figure 2c). The volcanic stratigraphic column was established using field observations, petrographic descriptions, geochemical characteristics, and geochronology (Figure 2d). The overall volcanic sequence in the Dera-Sire section is approximately 900m thick, extending from the Keleta River to the top of the escarpment (Figure 2b and d). From bottom to top, the volcanic sequence is lower basalt, lower ignimbrite, tuff and ash, upper basalt, and upper ignimbrite. The petrographic and geochemical results of the lower and upper basalts of the Dera-Sire section exhibit two distinct mineralogical and geochemical basaltic groups. The lower basalt is plagioclase-olivine phyric, and the upper basalt is aphric to sparsely plagioclase phyric. Based on geochemical classification, the lower and upper basalts are alkali and tholeiitic, respectively. The mineralogical and geochemical variations between the two groups may reflect variable magmatic evolution processes, contributions of crustal materials, and different mantle sources. Therefore, possible causes for the compositional variations of the lower and upper basalts are discussed below.

### 5.1. Role of fractional crystallization and degree of partial melting

The concentrations of Ni and Cr of the lower basalts (Cr =15.42-33.26 ppm and Ni = 32.56-42.71 ppm) and upper basalts (Ni =19.53-23.6 ppm and Cr =14.15-53.21 ppm) contents with low MgO values (3.08-5.9 wt %) are lower than the ranges of primary magma (Ni > 400–500 ppm), (Cr > 1000 ppm), and MgO (10-15 wt. %),[44] in equilibrium with a typical upper mantle mineral assemblage [45], showing that both lower and upper basalts are highly fractionated. The major and trace element variation diagrams show two distinct compositions, one for the lower basalt and the other for the upper basalt (Figures 8 and 9). $Al_2O_3$ is positively correlated with MgO in the lower basalt, possibly indicating the fractionation of plagioclase and olivine, which is a typical fractionation feature in the alkali and transitional magmatic series. Petrographic studies (Fig. 3) also indicate that the lower basalts are dominated by fractionated plagioclase and olivine phenocrysts. $Al_2O_3$ versus MgO in the upper basalt shows a negative trend, indicating that there are no plagioclase fractionations. The ratio $CaO/Al_2O_3$ decreases with a decrease in MgO for the lower basalt along the clinopyroxene fractionation trend, probably suggesting fractionation of clinopyroxene. The $CaO/Al_2O_3$ ratio showed a slight decrease with a decrease in MgO for the upper basalt, indicating minor clinopyroxene fractionation.

$TiO_2$ versus MgO displays constant trends in the upper basalts (Figure 8), indicating that there was no titanomagnetite fractionation. Although the lower basalt displays higher $TiO_2$ than the upper basalt, there is no clear fractionation trend observed in Figure 8, which also indicates that there is no titanomagnetite fractionation in the lower basalts. The petrographic descriptions indicate that opaque minerals are observed only as groundmasses in both groups, which also supports the above inference of no titanomagnetite fractionation. V is positively correlated with MgO in both basaltic groups, possibly indicating clinopyroxene fractionation. Even though the basaltic groups cannot be co-magmatic because of their time gaps, there is a possibility that they originated from similar mantle sources that melted during different periods. However, the observed compositional variations between the lower and upper basalts cannot be explained by fractional crystallization alone. As shown in Figure 11, the upper basalts show higher Rb/Nb and Zr/Nb ratios than

the lower basalts. This indicates a variation in the degree of partial melting, with the upper basalts formed by a higher degree of partial melting than the lower basalts.

### 5.2. Effect of Crustal Contamination

The Nb/Th ratio of oceanic basalt is 12-19 [42], and the continental crust Nb/Th ratio is ~1.42 [46]. Therefore, the Nb/Th ratios of the upper basalts (~ 9) and the lower basalts (9.7–11.1) are closer to the range of mantle-derived oceanic basalts and very far from the value of continental crust, implying that both the lower and upper basalts are affected by insignificant crustal materials. Ba/Nb ratio is an effective trace element ratio for assessing potential contamination by crustal materials, where the ratio of Ba/Nb values for crustal materials is 54 and mantle-derived oceanic basalt ranges from Ba/Nb (4.3–17.8) (Weaver, 1991). Thus, the observed values of the lower basalts Ba/Nb = 24.4–38.9 and the upper basalts Ba/Nb = 36.9–38.5 reflect minor crustal contamination in the genesis of both groups of basalt. As shown in K/Nb versus Th/Nb and Zr/Nb versus K/Nb (Figure 11c and d), both upper and lower basalts plot far from typical upper and lower continental crust values [47, 48], implying that both lower and upper basalts were insignificantly affected by crustal materials. Therefore, the incompatible trace element evidence indicates that crustal contamination cannot be considered the major controlling factor for the geochemical variations observed in both the upper and lower basalts.

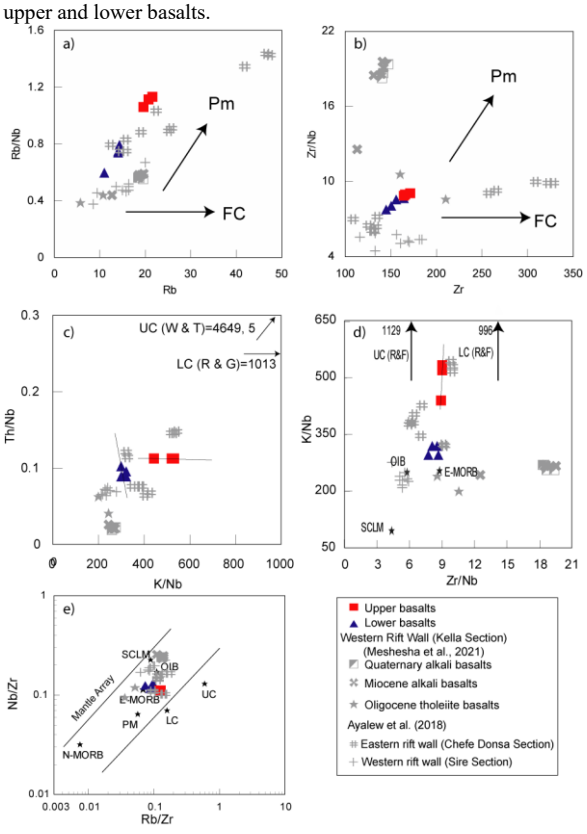


Figure 11 Selected highly incompatible trace element and ratio plots a) Rb vs. Rb/Nb, b) Zr vs. Zr/Nb, c) K/Nb vs. Th/Nb, d) Zr/Nb vs. K/Nb and e) Rb/Zr vs. Nb/Zr. Data for Western (Chefe Donsa Section) and Eastern Rift Wall (Sire Section) [38], Western Rift Wall (Kella Section) [39] are plotted for comparison. OIB, E-MORB, N-MORB and primitive mantle (PM) values from Sun and McDonough [42]. Reference values for upper crust (UC) and lower crust (LC) are taken from (R&F) [47, 48].

### 5.3. Mantle Source Variations

As shown in Figure 10c, the primitive mantle-normalized patterns of the upper and lower basalts are slightly lower than those of the OIB-type and higher than those of the E-MORB [42]. In terms of large ion lithophile elements and high field strength elements, both the upper and lower basalts show more enrichment than N-MORB [42]. The upper basalts are enriched in Nb, Ba, and Rb relative to the lower basalts.

As shown in Figure 11e, Rb/Zr versus Nb/Zr is used to discriminate between mantle end-members involved in the genesis of the upper and lower basalts. Both the upper and lower basalts plot within the mantle array, and most of the data plot between the OIB and E-MORB end-members. The upper basalts are characterized by a higher Rb/Zr ratio than the lower basalts. Neither the upper nor the lower basalts showed any interaction with crustal contaminants.

As shown in Figure 11e, at least two mantle components are required to produce both the lower (alkaline basalts, Oligocene in age) and upper basalts (tholeiitic basalts, Pliocene in age). These components are an OIB-like component [42], which might be similar to the Afar plume composition and an E-MORB-like component in the asthenosphere [42]. Based on the above discussion, there were no temporal mantle source variations from Oligocene to Pliocene magma generation. However, the alkaline nature of the lower basalt and the tholeiitic nature of the upper basalt suggest that the depth of melting of the lower basalt during the Oligocene is relatively deeper than that of the upper basalts in the Pliocene.

### 5.4. Petro-Stratigraphy and Magma Plumbing System

The discussion of petrostratigraphy and magma plumbing is constrained by the petrographic and geochemical results of the Dera-Sire section along the eastern MER escarpment (Figure 2). This discussion addresses the magmatic evolution inferred from the dominant phenocryst and microphenocryst mineral assemblages in a given flow with an assumed depth of fractionation and magnitude of magma flux into the lithosphere. Similarly, the phyric and aphyric textural differences among the volcanic units in the stratigraphic succession of the Dera-Sire section also provide clues for understanding the behaviour of the magmatic plumbing system.

Textural arrangements, zoning in plagioclase, and a wide range of phenocryst phase variations are very common in the described volcanic rocks, and these suggest a fractional crystallization history of the magma. The crystal shape of the minerals further supports the above assertion, with euhedral and subhedral minerals forming first, and anhedral crystals crystallizing later, providing insight into the formation of the volcanic products in the stratigraphic succession.

The lower basalts (alkaline basalts, Oligocene) display a modal percentage of up to 2-5% phenocrysts of plagioclase as the main phase, followed by olivine (1-3%), and minor clinopyroxene (< 1%).

Plagioclase phenocrysts have euhedral to subhedral shapes with tabular and elongated phenocrysts within the intergranular to microcrystalline groundmass. The olivine phenocrysts have subhedral shapes. Minerals such as plagioclase laths, olivine, clinopyroxene, and opaque minerals with intergranular texture constitute the groundmass. The overall mineralogical assemblage of the lower basalts is plagioclase-olivine-minor clinopyroxene.

The upper basalt (tholeiitic basalts, Pliocene) consisted of aphyric and sparsely plagioclase phyric basalts. The plagioclase phyric basalts display a modal percentage of up to 6% plagioclase phenocrysts as the main phase with minor olivine and clinopyroxene. The plagioclase phenocrysts show twinning and zoning. It is characterized by euhedral to subhedral shapes and tabular and elongated crystals within the intergranular to microcrystalline groundmass. Plagioclase laths with olivine, clinopyroxene, and opaque minerals constitute the groundmass.

Both the lower and upper ignimbrites contain 5–15% quartz crystals, alkali feldspar (dominant sanidine with minor orthoclase), plagioclase, and opaque minerals. The groundmass of ignimbrite is composed of microlites of similar minerals embedded in a glassy matrix (vitrophyric texture). At places, the lower ignimbrite samples consist of crystals of quartz and feldspar together with flattened and compacted glass shards displaying a eutaxitic texture and rock fragments of basaltic composition.

Based on the above petrographic discussion of the volcanic rocks in the Dera-Sire section, we envisaged the following scenario to explain the magma plumbing system (Fig. 12): The major crystallization phases of the lower basalts are plagioclase, olivine, and minor clinopyroxene minerals. The presence of olivine and minor clinopyroxene phenocrysts in the lower basalts suggests that the mantle-derived magma passed through the lithospheric mantle, accumulated in the lower crust (lower crustal chamber), and fractionated there. Then, the fractionated magma from the lower crustal chamber rose directly to the surface and produced lower basalts during the Oligocene.

The lower ignimbrites and tuff and ash units, which are silicic in composition, are possibly produced by 1) fractional crystallization and crustal assimilation, and 2) crustal melts or remelting of partially solidified magma caused by the high influx of magma that produced the lower basalts. The presence of paleosol between the lower basalts and lower ignimbrites indicates a hiatus between the two stratigraphic units.

The upper basalt (tholeiitic basalts, Pliocene) consisted of aphyric and sparsely plagioclase phyric basalts. The major crystallization phases of the sparsely phyric upper basalts are plagioclase and minor clinopyroxene. According to Morse (1980) and Krans et al. (2018), plagioclase crystallizes over clinopyroxene at a lower pressure (<5 kbar). From this mineral assemblage, we suggest that mantle-derived magma passed through the lithospheric mantle, accumulated in the upper crust (upper crustal chamber), and fractionated there. Then, the fractionated magma from the upper crustal chamber directly rises to the surface and episodically produces Pliocene phyric upper basalts. In contrast, the aphyric texture in the upper basalts may indicate a substantial influx of magma into the plumbing system, which caused the magma to rise to the surface without settling in the upper crustal chamber to produce aphyric verities in the upper basalts.

The upper ignimbrite was also produced under conditions similar to those of the lower ignimbrite, caused by the high influx of magma that produced the upper basalts. The presence of paleosol between the upper basalts and upper ignimbrite indicates that there is also a hiatus between the two stratigraphic units.

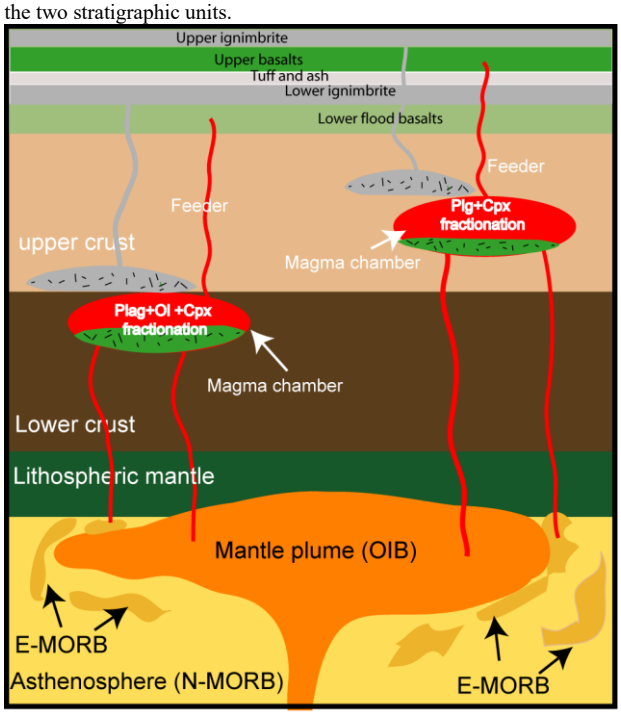


Figure 12. Simplified cartoon showing mantle source components and plumbing model of Dera-Sire section.

## 6. Conclusions

Field observations, petrographic, and geochemical investigations are conducted in the Dera-Sire volcanic section, the eastern escarpment of the central Main Ethiopian Rift. Stratigraphically, the Dera-Sire section consists of different units from bottom to top: lower flood basalt (Oligocene); lower ignimbrite, tuff, and ash; upper basalt (Pliocene); and upper ignimbrite, separated by paleosols.

Petrographically, the lower basalt is characterized by phyric in texture. The phenocrysts are composed of plagioclase, olivine, and minor clinopyroxene within the groundmass of microcrystalline plagioclase laths and opaque minerals. The lower ignimbrite contains quartz, plagioclase crystals and lithic fragments embedded within a glassy groundmass. The upper basalts are aphyric to sparsely phyric basalts, with a mineral assemblage of dominant plagioclase and minor clinopyroxene. The upper ignimbrite unit is composed of quartz crystals and lithic fragments of basaltic and pumice sets in a glassy matrix. The matrix is characterized using glass shards.

Geochemically, the lower basalts are alkaline in composition, whereas the upper basalts are sub-alkaline (tholeiite) in composition. The lower and upper basalts show two distinct compositions in the variation plots of the major oxide and trace elements. The observed compositional variations between the lower and upper basalts cannot be explained by the fractional crystallization process or crustal contamination. The geochemical variations suggest that at least two dominant mantle source components are required to produce both lower and upper basalts. The components are an OIB-like component, which might be similar to the Afar plume composition, and an E-MORB-like component in the asthenosphere, indicating that there was no temporal mantle source variation from the Oligocene to Pliocene magma generations. However, the alkaline affinity of the lower and tholeiitic nature of the upper basalts suggests that the melting depth of the lower basalt is relatively deeper than that of the upper basalts. From the presence of olivine and minor clinopyroxene phenocrysts in the lower basalts, it is suggested that mantle-derived magma accumulated in the lower crust and fractionated before eruption. Then, the fractionated magma from the lower crustal chamber rose directly to the surface and produced lower basalts in the Oligocene. However, from the major crystallization phases of the upper basalts, it is suggested that mantle-derived magma accumulated in the upper crust and fractionated before eruption in the Pliocene.

## Acknowledgement

The authors thank AASTU for research support, the Geological Institute of Ethiopia for thin section preparation, and Arba Minch University for geochemical analyses.

## References

[1] A. Davidson, D. Rex, Age of volcanism and rifting in southwestern Ethiopia, Nature 283(5748) (1980) 657-658.

[2] C. Ebinger, T. Yemane, G. Woldegabriel, J. Aronson, R. Walter, Late Eocene–Recent volcanism and faulting in the southern main Ethiopian rift, Journal of the Geological Society 150(1) (1993) 99-108.

[3] R. George, N. Rogers, S. Kelley, Earliest magmatism in Ethiopia: evidence for two mantle plumes in one flood basalt province, Geology 26(10) (1998) 923-926.

[4] R. Pik, C. Deniel, C. Coulon, G. Yirgu, C. Hofmann, D. Ayalew, The northwestern Ethiopian Plateau flood basalts: classification and spatial distribution of magma types, Journal of Volcanology and geothermal Research 81(1-2) (1998) 91-111.

[5] R. Pik, C. Deniel, C. Coulon, G. Yirgu, B. Marty, Isotopic and trace element signatures of Ethiopian flood basalts: evidence for plume–lithosphere interactions, Geochimica et Cosmochimica Acta 63(15) (1999) 2263-2279.

[6] B. Kieffer, N. Arndt, H. Lapierre, F. Bastien, D. Bosch, A. Pecher, G. Yirgu, D. Ayalew, D. Weis, D.A. Jerram, Flood and shield basalts from Ethiopia: magmas from the African superswell, Journal of Petrology 45(4) (2004) 793-834.

[7] C.J. Ebinger, N. Sleep, Cenozoic magmatism throughout east Africa resulting from impact of a single plume, Nature 395(6704) (1998) 788-791.

[8] N. Rogers, R. Macdonald, J.G. Fitton, R. George, M. Smith, B. Barreiro, Two mantle plumes beneath the East African rift system: Sr, Nd and Pb isotope evidence from Kenya Rift basalts, Earth and Planetary Science Letters 176(3-4) (2000) 387-400.

[9] T. Furman, J.G. Bryce, J. Karson, A. Iotti, East African Rift System (EARS) plume structure: insights from Quaternary mafic lavas of Turkana, Kenya, Journal of Petrology 45(5) (2004) 1069-1088.

[10] N. Rogers, Basaltic magmatism and the geodynamics of the East African Rift System, (2006).

[11] R. Pik, B. Marty, D. Hilton, How many mantle plumes in Africa? The geochemical point of view, Chemical Geology 226(3-4) (2006) 100-114.

[12] P. Mohr, The Morton-Black hypothesis for the thinning of continental crust—revisited in western Afar, Developments in Geotectonics, Elsevier1983, pp. 509-528.

[13] P. Mohr, B. Zanettin, The Ethiopian flood basalt province. Continental Flood Basalts 63–110, 1988.

[14] G. Yirgu, Magma-crust interaction during emplacement of Cenozoic volcanism in Ethiopia: geochemical evidence from Sheno-Magezez area Central Ethiopia, SINET: Ethiopian Journal of Science 20(1) (1997) 49-72.

[15] J. Baker, L. Snee, M. Menzies, A brief Oligocene period of flood volcanism in Yemen: implications for the duration and rate of continental flood volcanism at the Afro-Arabian triple junction, Earth and Planetary Science Letters 138(1-4) (1996) 39-55.

[16] C. Hofmann, V. Courtillot, G. Feraud, P. Rochette, G. Yirgu, E. Ketefo, R. Pik, Timing of the Ethiopian flood basalt event and implications for plume birth and global change, Nature 389(6653) (1997) 838-841.

[17] D. Meshesha, R. Shinjo, Crustal contamination and diversity of magma sources in the northwestern Ethiopian volcanic province, Journal of Mineralogical and Petrological Sciences 102(5) (2007) 272-290.

[18] G. Corti, Continental rift evolution: from rift initiation to incipient break-up in the Main Ethiopian Rift, East Africa, Earth-science reviews 96(1-2) (2009) 1-53.

[19] L. Beccaluva, G. Bianchini, C. Natali, F. Siena, Continental flood basalts and mantle plumes: a case study of the Northern Ethiopian Plateau, Journal of Petrology 50(7) (2009) 1377-1403.

[20] G. Woldegabriel, J.L. Aronson, R.C. Walter, Geology, geochronology, and rift basin development in the central sector of the Main Ethiopia Rift, Geological Society of America Bulletin 102(4) (1990) 439-458.

[21] E. Wolfenden, C. Ebinger, G. Yirgu, A. Deino, D. Ayalew, Evolution of the northern Main Ethiopian rift: birth of a triple junction, Earth and Planetary Science Letters 224(1-2) (2004) 213-228.

[22] N. Hayward, C. Ebinger, Variations in the along-axis segmentation of the Afar Rift system, Tectonics 15(2) (1996) 244-257.

[23] T. Abebe, M.L. Balestrieri, G. Bigazzi, The central Main Ethiopian rift is younger than 8 Ma: Confirmation through apatite fission-track thermochronology, Terra nova 22(6) (2010) 470-476.

[24] A. Agostini, M. Bonini, G. Corti, F. Sani, P. Manetti, Distribution of quaternary deformation in the central Main Ethiopian Rift, East Africa, Tectonics 30(4) (2011).

[25] D. Ayalew, The relations between felsic and mafic volcanic rocks in continental flood basalts of Ethiopia: implication for the thermal weakening of the crust, (2011).
[26] B. Baker, P. Mohr, L. Williams, Geology of the eastern rift system of Africa. Geological Society of America; 1972.
[27] G. Merla, E. Abbate, A. Azzaroli, P. Bruni, M. Fazzuoli, M. Sagri, P. Tacconi, Geological map of Ethiopia and Somalia and comment, CNR, Firenze 7 (1979).
[28] V. Acocella, T. Korme, Holocene extension direction along the main Ethiopian Rift, East Africa, Terra nova 14(3) (2002) 191-197.
[29] J. Cochran, G. Karner, Constraints on the deformation and rupturing of continental lithosphere of the Red Sea: the transition from rifting to drifting, (2007).
[30] C. Morley, Early syn-rift igneous dike patterns, northern Kenya Rift (Turkana, Kenya): Implications for local and regional stresses, tectonics, and magma-structure interactions, Geosphere 16(3) (2020) 890-918.
[31] B. Abebe, V. Acocella, T. Korme, D. Ayalew, Quaternary faulting and volcanism in the Main Ethiopian Rift, Journal of African Earth Sciences 48(2-3) (2007) 115-124.
[32] I.A. Ukstins, P.R. Renne, E. Wolfenden, J. Baker, D. Ayalew, M. Menzies, Matching conjugate volcanic rifted margins: 40Ar/39Ar chrono-stratigraphy of pre-and syn-rift bimodal flood volcanism in Ethiopia and Yemen, Earth and Planetary Science Letters 198(3-4) (2002) 289-306.
[33] K. Stewart, N. Rogers, Mantle plume and lithosphere contributions to basalts from southern Ethiopia, Earth and Planetary Science Letters 139(1-2) (1996) 195-211.
[34] T. Chernet, W.K. Hart, J.L. Aronson, R.C. Walter, New age constraints on the timing of volcanism and tectonism in the northern Main Ethiopian Rift–southern Afar transition zone (Ethiopia), Journal of Volcanology and Geothermal Research 80(3-4) (1998) 267-280.
[35] C. Ebinger, T. Yemane, D. Harding, S. Tesfaye, S. Kelley, D. Rex, Rift deflection, migration, and propagation: Linkage of the Ethiopian and Eastern rifts, Africa, Geological Society of America Bulletin 112(2) (2000) 163-176.
[36] M. Bonini, G. Corti, F. Innocenti, P. Manetti, F. Mazzarini, T. Abebe, Z. Pecskay, Evolution of the Main Ethiopian Rift in the frame of Afar and Kenya rifts propagation, Tectonics 24(1) (2005).
[37] A. Peccerillo, M. Barberio, G. Yirgu, D. Ayalew, M. Barbieri, T. Wu, Relationships between mafic and peralkaline silicic magmatism in continental rift settings: a petrological, geochemical and isotopic study of the Gedemsa volcano, central Ethiopian rift, Journal of Petrology 44(11) (2003) 2003-2032.
[38] D. Ayalew, S. Jung, R. Romer, D. Garbe-Schönberg, Trace element systematics and Nd, Sr and Pb isotopes of Pliocene flood basalt magmas (Ethiopian rift): A case for Afar plume-lithosphere interaction, Chemical Geology 493 (2018) 172-188.
[39] D. Meshesha, T. Chekol, S. Negussia, Major and trace element compositions of basaltic lavas from western margin of central main Ethiopian rift: enriched asthenosphere vs. mantle plume contribution, Heliyon 7(12) (2021).
[40] M.L. Bas, R.L. Maitre, A. Streckeisen, B. Zanettin, I.S.o.t.S.o.I. Rocks, A chemical classification of volcanic rocks based on the total alkali-silica diagram, Journal of petrology 27(3) (1986) 745-750.
[41] T.N. Irvine, W. Baragar, A guide to the chemical classification of the common volcanic rocks, Canadian journal of earth sciences 8(5) (1971) 523-548.
[42] S.-S. Sun, W.F. McDonough, Chemical and isotopic systematics of oceanic basalts: implications for mantle composition and processes, Geological Society, London, Special Publications 42(1) (1989) 313-345.
[43] B.L. Weaver, The origin of ocean island basalt end-member compositions: trace element and isotopic constraints, Earth and planetary science letters 104(2-4) (1991) 381-397.
[44] F.A. Frey, M. Prinz, Ultramafic inclusions from San Carlos, Arizona: petrologic and geochemical data bearing on their petrogenesis, Earth and Planetary Science Letters 38(1) (1978) 129-176.
[45] D. Ayalew, S. Jung, R. Romer, F. Kersten, J. Pfänder, D. Garbe-Schönberg, Petrogenesis and origin of modern Ethiopian rift basalts: Constraints from isotope and trace element geochemistry, Lithos 258 (2016) 1-14.
[46] R.L. Rudnick, H.D. Holland, R.L. Rudnick, The crust, Elsevier2005.
[47] R.L. Rudnick, D.M. Fountain, Nature and composition of the continental crust: a lower crustal perspective, Reviews of geophysics 33(3) (1995) 267-309.
[48] B.L. Weaver, J. Tarney, Empirical approach to estimating the composition of the continental crust, Nature 310(5978) (1984) 575-577.